J. Fluid Mech. (1969), *vol.* 38, *part* 2, *pp.* 375–400
Printed in Great Britain

The effect of horizontal gradients on thermohaline convection

By S. A. THORPE, P. K. HUTT† AND R. SOULSBY‡
National Institute of Oceanography, Wormley, Godalming, Surrey

(Received 28 February 1969)

When the vertical boundaries of a container of stratified brine solution are heated, cells are observed to form in the brine with a layered structure. An explanation of this phenomenon has been given in terms of the successive growth of cells from the top and bottom of the container. An alternative explanation is given here which is based on an examination of the stability of the fluid layer in the neighbourhood of the vertical boundaries, a layer in which there exist horizontal gradients in both temperature and salinity, and the explanation is subjected to comparison with a carefully controlled laboratory experiment. The theoretical description is fairly general and it seems possible that the effects of horizontal gradients of salinity and temperature, which approximately compensate each other so as to leave no horizontal density gradient, may be important in the ocean, as suggested by Stern (1967).

1. Introduction

In the early experiments by Turner & Stommel (1964) in which a stably stratified brine solution was heated from below, layers were observed both near the bottom of the container and further up. The layers near the bottom grew successively one on top of the other, and an explanation of these layers has been given both in the original paper and also later in greater detail by Turner (1968). The layers further up the container were explained as being due to heat entering through the side walls, being similar in nature to those found in the subsidence of suspension of fine particles in a tube which were observed and explained by Mendenhall & Mason (1923). Similar layers were observed in the experiment in a stratified brine solution by Thorpe (1966) and figure 1, plate 1, shows how they develop. To the left of the photographs is a brine solution with a uniform stable salinity gradient. A small crystal of potassium permanganate is fixed near to the vertical wall of the container and dye from the crystal colours the layers which appear some time after the wall is first heated. (The dye plays no part in the phenomenon; the layers develop in exactly the same way if no dye is used and a shadowgraph technique is used for observation.) The layers first appear as a series of two-dimensional rolls near the wall, in each of which there is a counter-clockwise

† Present address: Trinity College, Cambridge.
‡ Present address: Marine Science Laboratories, Menai Bridge, Anglesey.

rotation (so that fluid rises near the hot wall). The width of these rolls increases quite rapidly to form layers with a slight downward inclination. Some of them amalgamate, usually by fluid from a lower layer penetrating through its upper boundary near the hot wall into the cell above and then taking part in the motion in the upper layer. The layers are observed to increase their horizontal scale until they reach the further wall of the container, still maintaining clear boundaries between each of them. Provided the lateral walls are well insulated the motions appear to be quite two-dimensional. A description of the developed layers in a typical experiment is given in § 4, and figure 11, plate 2, shows the appearance of the layers some time after they had spread right across the rectangular container.

The explanation offered by Thorpe (1966) for the formation of the layers was essentially that of Mendenhall & Mason applied to a heated side-wall rather than a cooled one. Mendenhall & Mason's explanation is, for convenience, reprinted below:

> Suppose now that the temperature of one side of the tube be lowered so that a lateral difference of temperature is established across the tube at all levels. If no vertical density variation were present, the liquid would be set into convection, the entire volume of the liquid furnishing a single continuous convective pattern, with lines of flow near the wall which would extend continuously from top to bottom on the cold side and from bottom to top on the hot side. If a sufficient density gradient due to suspended particles be initially present in the liquid, however, a different type of convection will be formed. A portion of the liquid near the cold wall becomes denser than the average at its depth and flows downwards. As it falls, its negative buoyancy due to temperature difference becomes continuously less since the density of the liquid into which the portion is flowing is greater on account of its larger content of suspended particles. Reaching a level where its temperature contraction balances the excess density of the main mass of fluid at that depth it is in stable equilibrium, and the downward flow ceases. Fluid elements near the cold wall thus tend to flow a definite distance downwards.
>
> As the uppermost element A moves down, fluid from the top of the column follows in its wake, so that while the elements below A show variation in density due to particle content, the new elements which are continuously brought to the top of the cold wall are drawn from the top portion of the liquid and are of nearly uniform density.
>
> When A reaches its equilibrium depth, its downward flow is decelerated and it turns into the interior of the liquid, this motion being followed by the elements behind A. The equilibrium depth for A thus acts approximately as a boundary limiting the flow, and a local convection is established in the upper portion of liquid, this portion being mixed so that its particle content becomes uniform, equal to the average content of the portion before mixing. Thus a definite upper layer is formed, with an internal convection system, the density being uniform and less than that of the liquid below.
>
> The bottom of this layer acts for the fluid below it, as did the top surface of the liquid in the formation of the top layer. A second layer establishes itself, similar in character to the top layer, and in this manner the entire volume of liquid is divided into layers.
>
> The layer depth is characterized by the fact that the thermal contraction of the fluid elements originally at its top is sufficient to increase the density to that originally obtaining at its bottom, due to the increased content of suspended particles.

This explanation rests on the assumption that the layers grow in succession, one on top of the other, from the horizontal boundaries of the fluid, and it does not supply any lower bound on the temperature contrasts required to produce layers. Experiments with stratified brine solution show that indeed the first appearance of layers is near the horizontal boundaries, sometimes at both top and bottom of the container, but that the layers at intermediate levels can grow *simultaneously*, and not in succession from the horizontal boundaries. This observation has been carefully confirmed by means of time-lapse photography. Moreover, it is observed that small increases in wall temperature do not lead to the simultaneous formation of layers, at least in the time during which the experiments were made (up to 90 min), whereas larger increases produce layers quite rapidly. In the experiments which will be described in § 3, the stratified brine solution is contained between two vertical walls separated by a small distance, and the temperature difference between the two walls just sufficient to produce the layers, is not found to be subject to the rate at which the fluid is heated.

It is suggested that the first appearance of layers near the horizontal boundaries of the fluid may be due either to the effects described by Mendenhall & Mason, or to the fact that the vertical gradients of salinity in these regions are smaller than at other layers (there being no salt flux through the boundaries, the salt gradients must fall to zero), so that the fluid is less stable in these regions in the sense described below. Further it is suggested that the layers growing simultaneously at intermediate depths are the result of a difference in the diffusivities of heat and salinity and the presence of horizontal gradients of temperature and salinity near the vertical wall. Near a heated wall the fluid, becoming warmer by conduction, will tend to rise under buoyancy forces, but will not change its salinity very much, owing to the very small value of the coefficient of diffusivity of salinity, and thus horizontal salinity gradients, as well as temperature gradients, will be established. If the heating is carried out sufficiently slowly the horizontal density gradient will at all times be very small (and it will be neglected in the theoretical discussion). It will be shown below that the presence of sufficiently large horizontal gradients will lead to instability with a layered structure. Cells will grow simultaneously only when the heating is such that these sufficiently large gradients are achieved.

The simplest physical illustration of the instability is to consider two fluid particles lying at the same horizontal level in a fluid containing no vertical gradients, but horizontal gradients of temperature and salinity which just compensate so that there is no horizontal density gradient. If the particles of fluid are interchanged, the particle introduced into warmer and saltier surroundings becomes warmer but not much saltier, since the coefficient of diffusion of heat is about one hundred times greater than that of salinity, and it therefore rises, being less dense than its salty surroundings, whilst the other particle sinks. Thus we have generated *vorticity* in the fluid, and this is the source of the instability. This physical argument ignores viscosity and vertical gradients which play their part in providing a criterion for the onset of instability.

In order to establish a length scale, both theory and the experiments have been made in a fluid bounded by parallel planes, the length scale being the separation

between these planes, and only constant gradients of salinity and temperature are considered. In the case of a broad container heated through a vertical boundary, the length scale is provided by the thickness of the heated layer near the wall, and the length scale of the layers when they first appear, and the characteristics of the motion, will usually depend on the heated-layer thickness and also upon the rate at which the fluid is heated, just as is the case in the Bénard problem (Currie 1967).

A linear theory designed to predict the onset of instability, but not the details of the finite-amplitude flows which follow, is described in § 2. Only situations in which the marginal state is characterized by the onset of steady convective motions are examined. This theory extends existing results by Stern (1960), Walin (1964), Veronis (1965) and Nield (1967) on thermohaline convection with vertical gradients. The boundary conditions satisfied by the particular solution chosen for examination are not ones which would be satisfied in practice, but the additional calculations required to treat realistic boundary conditions are formidable, and are not attempted here. Emphasis is placed on the theory which relates to the experiments discussed in § 3, and the theoretical and experimental results compare well, somewhat better than was to be expected in view of the boundary conditions used.

The results and conclusions are summarized in § 5 and their application to the occurrence of the layers which have been observed in the deep ocean is discussed.

2. Theory

We consider a fluid lying at rest between parallel planes inclined at an angle γ to the horizontal, and separated by a distance d (see figure 2). The x axis and y axis are horizontal, the y axis (not shown in the figure) lying in the lower bounding plane, and the z axis is vertically upwards. The equation of state in the fluid is taken to be

$$\rho = \rho_0(1-\alpha\theta+\beta S), \tag{1}$$

where ρ is the density, ρ_0 is a constant density, θ is the temperature and S the salinity, α is the coefficient of expansion and β is the coefficient representing the proportional density change for unit change in salinity at constant temperature. Both α and β are supposed to be constant and positive. In the undisturbed state the fluid contains uniform horizontal and vertical temperature gradients, $\nabla\theta_0 = (\theta_{0x}, 0, \theta_{0z})$, and salinity gradients, $\nabla S_0 = (S_{0x}, 0, S_{0z})$, such that the horizontal density gradient is zero, so that

$$\alpha\theta_{0x} = \beta S_{0x}, \tag{2}$$

and the vertical density gradient negative (or zero), so that

$$\beta S_{0z} - \alpha\theta_{0z} \leqslant 0, \tag{3}$$

and the fluid is stably stratified (or neutral). The boundary conditions in this basic state are such that walls match the temperature and salinity conditions in the fluid. We consider a small perturbation of this state.

The equations which govern the motion are

continuity: $$\nabla . \mathbf{u} = 0; \tag{4}$$

vorticity: $$\frac{\partial \boldsymbol{\omega}}{\partial t} + \mathbf{u} . \nabla \boldsymbol{\omega} - \boldsymbol{\omega} . \nabla \mathbf{u} = \nu \nabla^2 \boldsymbol{\omega} - \frac{g}{\rho_0} \nabla \times (\rho \nabla z); \tag{5}$$

temperature: $$\frac{\partial \theta}{\partial t} + \mathbf{u} . \nabla \theta = K_\theta \nabla^2 \theta; \tag{6}$$

salinity: $$\frac{\partial S}{\partial t} + \mathbf{u} . \nabla S = K_s \nabla^2 S; \tag{7}$$

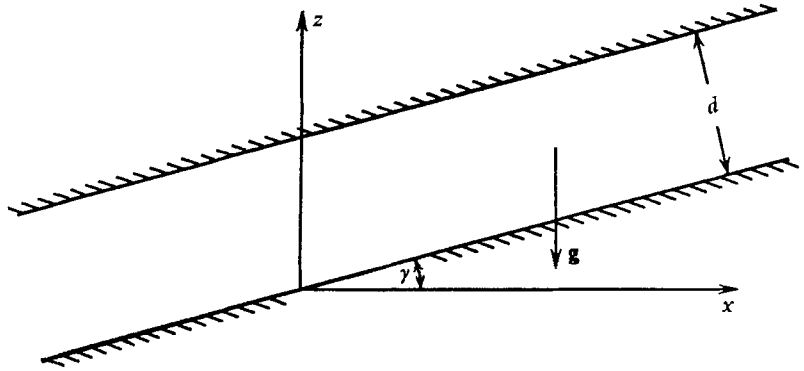

FIGURE 2. Notation.

where $\mathbf{u}$ is the velocity, $\boldsymbol{\omega} = \nabla \times \mathbf{u}$ is the vorticity, ν is the coefficient of kinematic viscosity, K_θ is the coefficient of thermal diffusivity and K_s is the coefficient of diffusion of salinity. All the coefficients, ν, K_θ and K_s, are supposed constant. In equation (5), the Boussinesq approximation has been made. (This approximation is valid in the experiments because of the small proportional differences in density which occur.) We shall suppose that the motion is confined to the (x, z) plane (this assumption is justified in appendix C for the type of solutions examined), so that there exists a stream function, ψ, with

$$\mathbf{u} \equiv (u, v, w) = (\psi_z, 0, -\psi_x). \tag{8}$$

We look for conditions in which the perturbation takes the form of steady motions. It is known that, in circumstances in which $S_{0z} < 0$, $\theta_{0z} < 0$ with $S_{0x} = \theta_{0x} = 0$, the onset of instability may be characterized by overstable motions, that is growing fluctuations (Veronis 1965). It appears that similar overstable motions will occur if S_{0x} and θ_{0x} are non-zero, and that the presence of horizontal gradients will tend to destabilize the motion, but these circumstances are not considered here. In the conditions which occur in the experiment, we have not been able to see how, on physical grounds, an overstable motion might occur, and the onset of instability is seen to take the form of convective rolls rather than overstable motions.

The linearized perturbation equations are

$$\nu\nabla_1^4\psi + g(\beta S_x - \alpha\theta_x) = 0, \tag{9}$$

$$S_{0x}\psi_z - S_{0z}\psi_x = K_s\nabla_1^2 S, \tag{10}$$

$$\theta_{0x}\psi_z - \theta_{0z}\psi_x = K_\theta\nabla_1^2\theta, \tag{11}$$

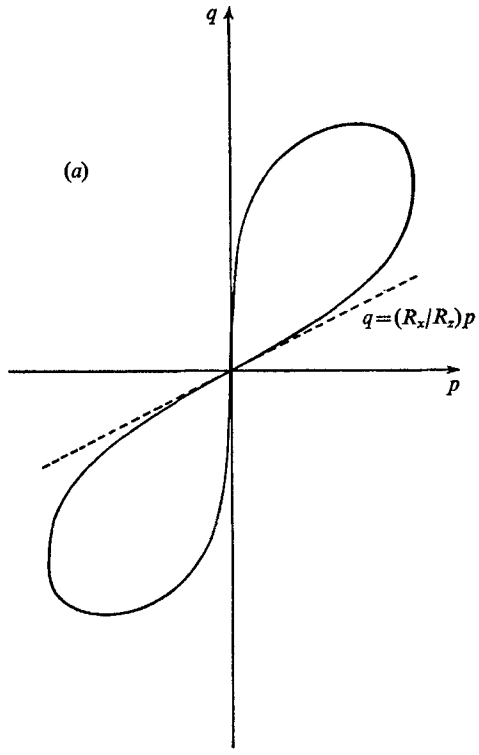

FIGURE 3. Sketch of the curve given by equation (17) for (a) $R_x < 0$, $R_z < 0$, (b) $R_x > 0$, $R_z < 0$.

where $\nabla_1^2 \equiv \partial^2/\partial x^2 + \partial^2/\partial z^2$, and θ and S are the perturbations in temperature and salinity, respectively. If we substitute from (10) and (11) into (9), we obtain an equation for the stream function,

$$\nabla_1^6\psi = \frac{g}{\nu}\left(\frac{\beta S_{0z}}{K_s} - \frac{\alpha\theta_{0z}}{K_\theta}\right)\psi_{xx} - \frac{g}{\nu}\left(\frac{\beta S_{0x}}{K_s} - \frac{\alpha\theta_{0x}}{K_\theta}\right)\psi_{xz}. \tag{12}$$

This equation, and (10) and (11), are to be solved subject to boundary conditions on the planes $z\cot\gamma - x = 0, d/\sin\gamma$. In an experiment the boundary conditions would be those of zero velocity at the planes, together with some appropriate conditions on salinity and temperature (for example, no salinity flux through the planes and the temperature maintained constant). Whilst it is desirable to apply such conditions, to do so is a considerable task and one which the value of the results might hardly justify; instead we select simple analytic solutions of (12) which satisfy the condition that there is no flow through the bounding planes,

and, for the moment, disregard what other boundary conditions may be satisfied. This inverse method has long been used in finding solutions for the Bénard problem which are unrealistic, in the sense that they do not satisfy boundary conditions which can be produced in the laboratory. It is possible that the general character of the flow is well predicted by such solutions, particularly when the wall boundary layers influence only a small part of the total flow. We shall discuss this point later in the context of the experiments.

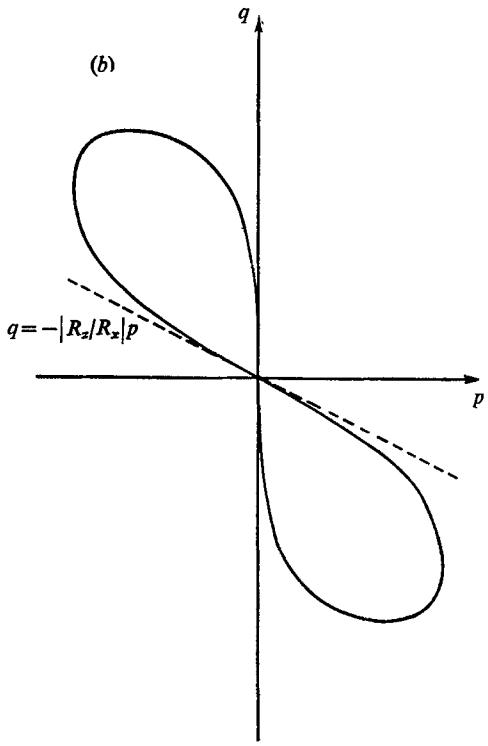

FIGURE 3(*b*). For legend see facing page.

A solution of (12) which satisfies the no-flow condition at the boundaries is

$$\begin{aligned}\psi &= 2\psi_0 \sin k(z\cot\gamma - x)\sin(lx+mz),\\ &= \psi_0\{\cos[(l+k)x+(m-k\cot\gamma)z]-\cos[(l-k)x+(m+k\cot\gamma)z]\},\end{aligned} \quad (13)$$

where ψ_0, k, l and m are constants, provided that $k = (n\pi\sin\gamma)/d$, where n is an integer, and

$$\begin{aligned}[(l\mp k)^2+(m\pm k\cot\gamma)^2]^3 = {}& \frac{g}{\nu}\left(\frac{\beta S_{0z}}{K_s}-\frac{\alpha\theta_{0z}}{K_\theta}\right)(l\mp k)^2\\ & -\frac{g}{\nu}\left(\beta\frac{S_{0x}}{K_s}-\frac{\alpha\theta_{0x}}{K_\theta}\right)(l\mp k)(m\pm k\cot\gamma).\end{aligned} \quad (14)$$

We now introduce non-dimensional variables by scaling x and z with

$$d/(n\pi\sin\gamma),$$

and (14) becomes

$$[(L\mp 1)^2+(M\pm\cot\gamma)^2]^3 = R_z(L\mp 1)^2 - R_x(L\mp 1)(M\pm\cot\gamma), \tag{15}$$

where

$$L=\frac{ld}{n\pi\sin\gamma},\quad M=\frac{md}{n\pi\sin\gamma},\quad R_x=\frac{gd^4\beta S_{0x}}{n^4\pi^4\sin^4\gamma\nu k_s}-\frac{gd^4\alpha\theta_{0x}}{n^4\pi^4\sin^4\gamma\nu K_\theta},$$

and

$$R_z=\frac{gd^4\beta S_{0z}}{n^4\pi^4\sin^4\gamma\nu K_s}-\frac{gd^4\alpha\theta_{0z}}{n^4\pi^4\sin^4\gamma\nu K_\theta}.$$

The expression

$$\frac{gd^4\alpha\theta_{0z}}{n^4\pi^4\sin^4\gamma\nu K_\theta}$$

has the form of a Rayleigh number, and parameters corresponding to this and

$$\frac{gd^4\alpha S_{0z}}{n^4\pi^4\sin^4\gamma\nu K_s}$$

have already appeared in the problems of thermohaline convection between horizontal parallel planes. Solutions of the equations (15) represent possible steady flows with a cellular pattern. In order to find out which of these flows will occur for given vertical gradients of salinity and temperature as the horizontal gradients are increased (but always satisfying (2)), it is necessary to find the minimum value of $|R_x|$ which satisfies (15), and the corresponding values of L and M, for a given value of R_z. The equations (15) are equivalent to

$$(p^2+q^2)^3 = R_z p^2 - R_x pq, \tag{16}$$

with origins displaced to $(-1,\cot\gamma)$ and $(1,-\cot\gamma)$. Equation (16) is parameterized by putting $q=ap$, so that

$$p^4=\frac{R_z-aR_x}{(1-a^2)^3},\quad q^4=a^4\frac{(R_z-aR_x)}{(1+a^2)^3} \tag{17}$$

(and $p=q=0$). This curve is shown diagrammatically for $R_x<0$, $R_z<0$ in figure 3(*a*) and for $R_x>0$, $R_z<0$ in figure 3(*b*).

In the (L,M) plane we have two such curves and the minimum value of R_x for which there are simultaneous solutions of (15) is, in general, that value of R_x for which the two curves first touch. This condition is generally difficult to obtain and we therefore examine in detail only the particular cases of interest $\gamma=\frac{1}{2}\pi$ and $\gamma=0$.

Case 1. $\gamma=\frac{1}{2}\pi$ (*vertical walls*)

The centres of the two curves are at $(\pm 1, 0)$ (see figure 4(*a*)). To a first approximation, the curves first touch when the left-hand curve touches the line $L=1$. From (17) we find that $dp/da=0$ when

$$(5a^2-1)R_x-6aR_z=0, \tag{18}$$

and the condition that the curve (17) touches $p=2$ is that (18) and $p=2$, that is

$$16(1+a^2)^3 = R_z-aR_x, \tag{19}$$

are satisfied simultaneously. Equations (18) and (19) can be written

$$\left.\begin{aligned} R_x &= -96a(1+a^2)^2, \\ R_z &= -16(5a^2-1)(1+a^2)^2, \end{aligned}\right\} \tag{20}$$

and this is a parametric form of the approximate stability curve in the (R_x, R_z) plane, which is sketched in figure 5. As $a \to \infty$, $(-R_x)$ and $(-R_z)$ both tend to infinity and $(-R_x) \to 2{\cdot}50(-R_z)^{\frac{5}{4}}$, whilst, when $a^2 = \frac{1}{5}$, $-R_x = 62$ and $R_z = 0$. (For $R_z \geqslant 1$, the curves in figure 4(*a*) may touch at $L = M = 0$ and solutions,

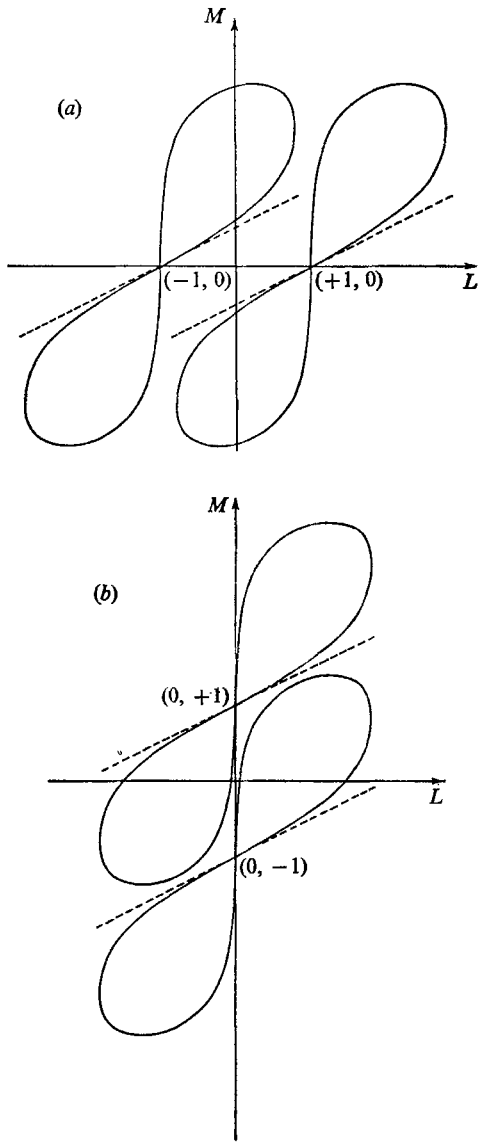

FIGURE 4. (*a*) Sketch of the curves representing the simultaneous equations (15) for $\gamma = \frac{1}{2}\pi$ and (*b*) equations (23) for $\gamma = 0$.

$\psi \propto \sin(m\pi x/d)$, independent of R_x may be found. However, solutions with $m = 1$ do not satisfy a condition of no mean vertical flux and the solution with $m = 2$ is equivalent to the solution $R_x = 0$, $R_z = 16$ shown in figure 5.)

Now $R_x = R_x^{(1)}/n^4$ and $R_z = R_z^{(1)}/n^4$ say, where $R_x^{(1)}$, $R_z^{(1)}$ are independent of n. The minimum horizontal gradients to produce steady motions (and therefore instability) are given by the minimum values of $|R_x^{(1)}|$ produced by varying n but keeping $R_z^{(1)}$ fixed.

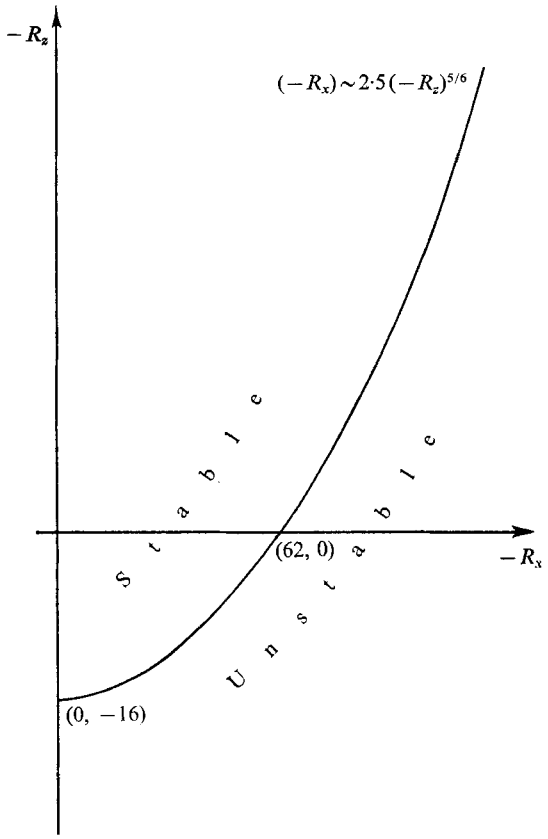

FIGURE 5. Sketch of the curve representing marginal stability for $\gamma = \frac{1}{2}\pi$.

Now from (20)

$$-R_x^{(1)} = 96n^4a(1+a^2) \quad \text{and} \quad (1/n^4)(-R_z^{(1)}) = 16(5a^2-1)(1+a^2)^2,$$

and it may easily be shown by differentiation with respect to n and substitution that

$$\frac{d}{dn}(-R_x^{(1)}) = 64\frac{n^3}{a}(1+a^2)^3, \quad > 0 \quad \text{if} \quad a > 0 \quad \text{and} \quad n > 0.$$

Hence the minimum horizontal gradients necessary for instability will produce a motion with $n = 1$ and the cells will reach right across the region between the vertical walls.

The approximation made in assuming that the curves in figure 4(*a*) touch when the left-hand curve touches the line $L = 1$ is found to be very good. In appendix A it is shown that the solution as $(-R_z) \to \infty$ is

$$\min |R_x| = 2{\cdot}76(-R_z)^{\frac{1}{3}}, \tag{21}$$

with
$$L = \sqrt{(\tfrac{3}{2})} \quad \text{and} \quad M = (-\tfrac{1}{2}R_z)^{\frac{1}{3}}. \tag{22}$$

In the experiments described in § 3, R_z will be large and negative, and the observations will be compared with the prediction (21) for the relative values of R_x and R_z at the onset of instability. In dimensional units

$$\psi = 2\psi_0 \sin\frac{\pi x}{d} \sin\left[\sqrt{\left(\frac{3}{2}\right)}\frac{\pi x}{d} + \left(-\frac{R_z}{2}\right)^{\frac{1}{3}}\frac{\pi z}{d}\right],$$

and the height of each cell is $d(-2/R_z)^{\frac{1}{3}}$, whilst the cell boundaries slope down at an angle $\tan^{-1}[(-27/4R_z)^{\frac{1}{3}}]$ to the horizontal. For $(-R_z) = 2 \times 10^4$, a value typical of the experiments, the cell height is $0{\cdot}215d$ and the slope of the cell boundary is about 15°. The cells corresponding to these values are shown in figure 6.

The solution for $R_z = 0$ is $\min|-R_x| = 63$,

with $L = 1{\cdot}01$ and $M = 0{\cdot}84$. These values agree very well with the approximate graphical solution given above.

The solution we have found is

$$\psi = 2\psi_0 \sin x \sin(LX + MZ)$$

(in non-dimensional parameters). At the boundaries $\psi = 0$, but neither first nor second derivative tends to zero. It is clear from (9) that a free choice of boundary conditions in this case for S and θ is impossible (for example, since $\nabla^4\psi = 0$ at the walls $X = 0$ and π, S_x and θ_x cannot both vanish there). In general it is possible to specify conditions on S (or θ) at both boundaries, but there is then little freedom of choice of conditions on θ (or S).

Case 2. $\gamma = 0$ (*horizontal boundaries*)

This case, in the absence of horizontal gradients, has been studied by Stern (1960), Veronis (1965) and Nield (1966). We avoid the singularity in $\cot\alpha$ by taking a solution of the form $\psi = \sin n\pi z/d \sin(lx + mz)$, and scale lengths with $d/n\pi$. Equation (15) now has the form

$$[L^2 + (M \pm 1)^2]^3 = R_z L^2 - R_x L(M \pm 1), \tag{23}$$

where
$$R_x = \frac{gd^4\beta S_{0x}}{n^4\pi^4\nu K_s} - \frac{gd^4\alpha\theta_{0x}}{n^4\pi^4\nu K_\theta}, \quad R_z = \frac{gd^4\beta S_{0z}}{n^4\pi^4\nu K_s} - \frac{gd^4\beta\theta_{0z}}{n^4\pi^4\nu K_\theta}.$$

The curves now have centres at $(0, \pm 1)$ and are shown in figure 4(*b*). An approximate condition that the curves touch is that the lower curve touches the line $M = 1 + (R_x/R_z)L$. Using the parametric form for the lower curve, the lower curve cuts this line where

$$(R_z - aR_x)^5 = 16(1 + a^2)^3 R_x^4. \tag{24}$$

This has a double root for a, that is the line touches the curve, if also

$$(R_z - aR_x)^4 = \tfrac{27}{5} a(1+a^2)^2(-R_x)^3. \tag{25}$$

Equations (24) and (25) may be re-written in the form

$$\left.\begin{aligned} -R_x &= 16\left(\frac{6a}{5}\right)^5 \frac{1}{(1+a^2)^2}, \\ -R_z &= \frac{16}{5}\left(\frac{6a}{5}\right)^4 \frac{(a^2-5)}{(1+a^2)^2}, \end{aligned}\right\} \tag{26}$$

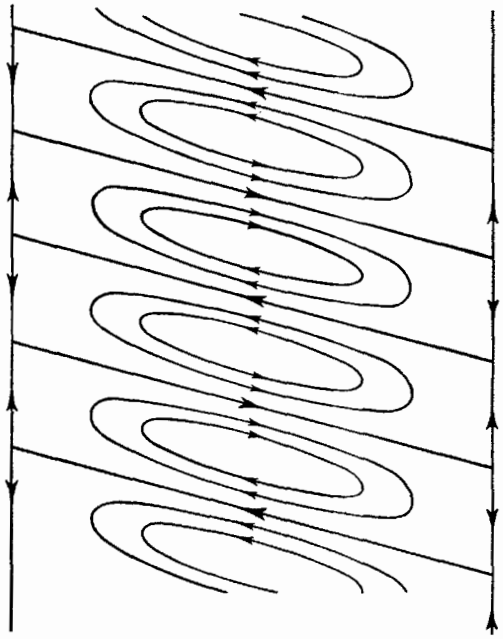

FIGURE 6. The shape of the cells predicted to form at the onset of convective instability for $(-R_z) = 2 \times 10^{-4}$ between vertical walls. The streamlines are marked for $\psi = 0$, $\psi = \frac{1}{2}\psi_0$ and $\psi = \psi_0$.

and this is a parametric representation of the stability curve (figure 7).

As $a \to \infty$, $(-R_x) \to \infty$ and $(-R_x) \sim 15{\cdot}4(-R_z)^{\frac{1}{2}}$, whilst, for $a^2 = 5$, $(-R_x) = 62$ and $R_z = 0$. The approximation breaks down when $a^2 < 5$. (For $R_x = 0$ convective motion first occurs when $R_z = 27/4$, see Veronis 1965.) As in case 1 it may easily be shown that the value of

$$(-R_x^{(1)}), = \frac{gd^4\alpha\theta_{0x}}{\pi^4\nu K_\theta} - \frac{gd^4\beta S_{0x}}{\pi^4\nu K_s},$$

increases as n increases for fixed $R_z^{(1)}$, and so the onset of instability is characterized by the solution with $n = 1$.

The approximations made in this graphical solution are found to be very good. In appendix B it is shown that, at the onset of instability, as $(-R_z) \to \infty$,

$$(-R_x) \sim 15{\cdot}6(-R_z)^{\frac{1}{2}} \tag{27}$$

with $$M = 1{\cdot}4, \quad L = 6{\cdot}2(-R_s)^{-\frac{1}{4}},$$

whilst for $R_s = 0$, $(-R_s) = 63$ with $M = 0{\cdot}84$, $L = 1{\cdot}01$.

The boundary conditions satisfied by the solution are similar to those found in case 1.

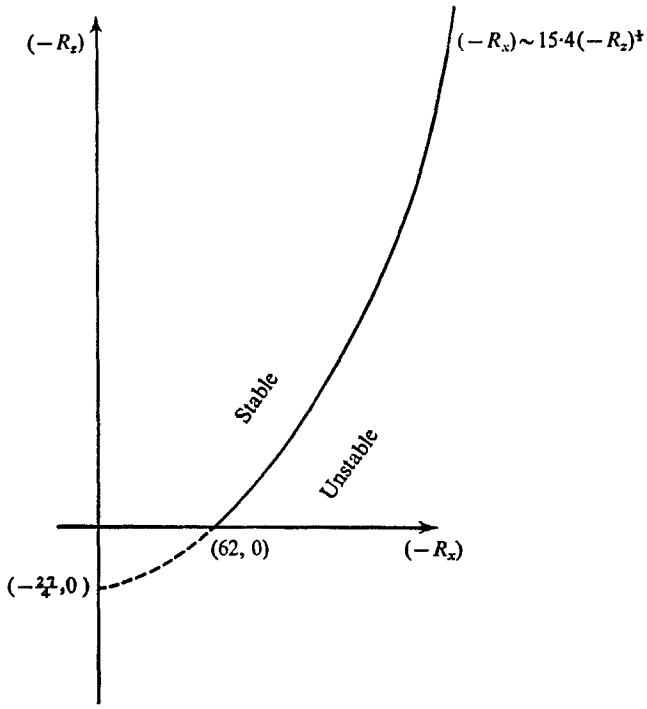

FIGURE 7. Sketch of the curve representing marginal stability for $\gamma = 0$.

3. Experiments

The experiments described below were designed to test the theoretical predictions for the case when the bounding walls are vertical ($\gamma = \frac{1}{2}\pi$) and the parameter R_s is large and negative.

The majority of the experiments were made in an apparatus consisting of a rectangular Perspex tank divided into three by two vertical brass plates each 1 mm thick and separated by 6 mm. The central section formed a narrow slot 6 mm wide, 15 cm deep and 7·5 cm broad, and the other wide sections were water baths. The tank walls were increased to a thickness of 1·86 cm in the slot region to avoid heating through these walls. (A few additional experiments were made in a slot 3·5 mm wide, 10·5 cm deep and 10·5 cm broad. The results of these experiments are shown in figures 9 and 10 by the points marked with crosses.) The whole tank was filled with brine with a uniform vertical salinity gradient produced by the method described by Oster (1965, see p. 74, 'Instant' density gradient). The brine was at room temperature, and the density gradients, corresponding to the salinity gradients, varied from 4×10^{-4} to $1{\cdot}52 \times 10^{-2}$ g cm^{-4}.

The slot was isolated from the filling device and from the neighbouring water baths, and small crystals of potassium permanganate were suspended on thin wires in the slot so as to produce traces by which to observe the fluid motions. Both water baths were then stirred continuously and their temperatures recorded every half minute. One of the baths was heated slowly,† the heating rate being controlled to a maximum of about 0·5 °C min^{-1} (usually much less). The use of a narrow slot and a slow rate of heating was an attempt to produce the conditions of the theory, namely uniform temperature gradient and zero density gradient across the slot. When one side of the slot is heated, vertical motions occur under buoyancy forces, which distort the salinity field so as to produce horizontal salinity gradients tending to restore the initial zero horizontal density gradient. The vertical temperature gradient is zero, and the initial vertical salinity gradient is always maintained in these motions. The conditions very close to the walls, at which a zero salinity-flux condition must be satisfied, are unlikely to be ideal, but over the major part of the width of the slot the heating rates are sufficiently small to produce suitable conditions for comparison with those envisaged in the theory. The rates of heating were reduced as the conditions were approached at which instability was, from earlier experience, to be expected, so as not to seriously overshoot the critical conditions. The temperature difference between the baths was held constant when instability was observed.

For small temperature differences between the vertical walls, maintained for up to 80 min, no instability was observed except near the top and bottom of the slot where one or two convective rolls were observed; however, when the temperature difference was sufficiently large, two-dimensional rolls were found to develop quite rapidly and apparently simultaneously in the slot well away from the horizontal boundaries. The rolls are shown in the photograph, figure 8, plate 2, in which the camera is pointed in a horizontal direction looking along the axes of the rolls in the plane bisecting the slot. The heated water bath is to the right of the photograph, and the cold bath to the left. The scale is in centimetres. The cells are well developed in two groups, but are only just becoming unstable in the very centre of the slot. The boundaries of the cells slope down to the left as predicted in the theory. It was noticed that the formation of cells was accompanied by a marked increase in the rate of heating of the colder water bath. For an initial vertical density gradient due to salinity of 1×10^{-4} g cm^{-4}, the temperature difference across the slot required to just produce rolls was about 2·3 °C and the cell height was 3·3 mm in the 6 mm wide slot. The maximum temperature differences found necessary to produce instability were 7 °C in the 6 mm slot and 9·5 °C in the 3·5 mm slot. Over such a large range of temperature the coefficients α, β, K_θ, K_s and ν are not constant as supposed in the theory, but may vary by up to about 10 %.‡ For this reason no larger salinity gradients, requiring correspondingly larger temperature differences to produce instability, were tried.

† Cooling one of the water baths was found to produce similar effects to those described here, but with cells orientated in the opposite direction as predicted by the theory. It was easier to arrange for controlled heating and for this reason the majority of experiments were made with one water bath heated.

‡ In figure 9 these coefficients appear effectively to the $\frac{1}{6}$ power and the variation is not significant.

It was noticed that, contrary to the predictions of the theory, the motions in all the cells have the same sense of rotation, with a motion up the heated wall and down the cold wall, so that motion in each cell is anticlockwise as seen in figure 8. It is suggested that this may be the result of exceeding the critical temperature difference required to first produce instability. The additional heating of the wall will tend to enhance the upward velocities and thus promote

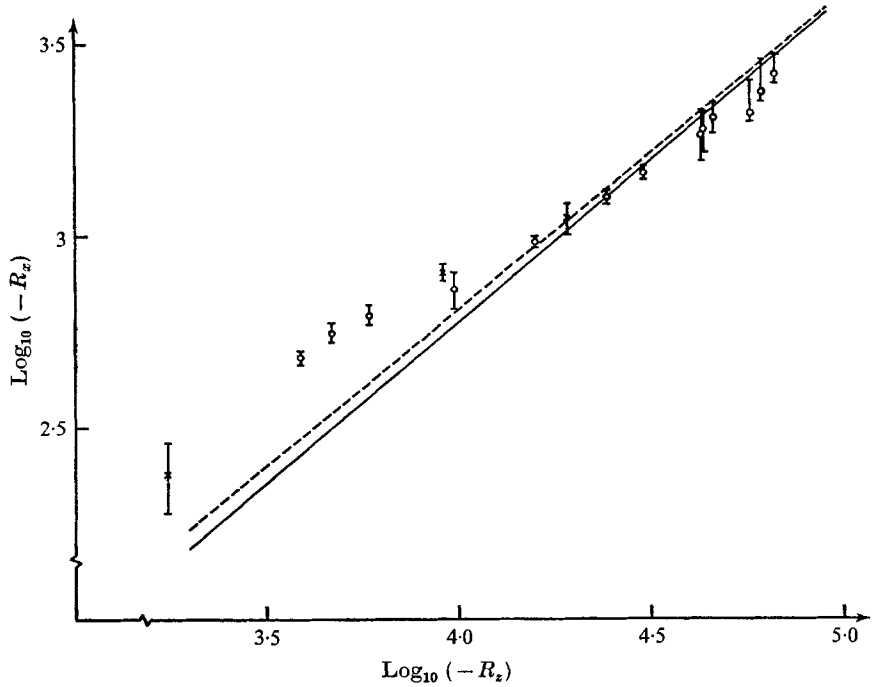

FIGURE 9. Plot of $\log_{10}(-R_x)$ against $\log_{10}(-R_z)$. The points represent observed values at the onset of instability for a 6 mm slot (O) and a 3·5 mm slot (×). The straight line represents the theoretical asymptotic curve at marginal stability and the dotted line the first-order correction.

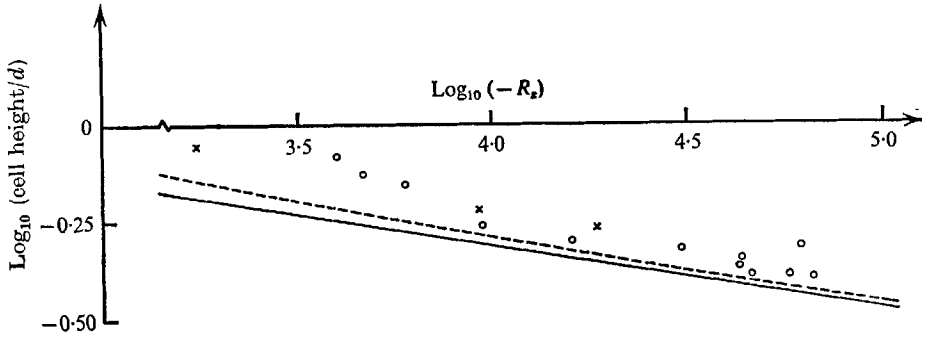

FIGURE 10. Plot of the logarithm of cell height divided by cell width against $\log_{10}(-R_z)$. The points represent the observed values at the onset of instability for a 6 mm slot (O) and a 3·5 mm slot (×). The straight line represents the theoretical asymptotic curve for large $(-R_z)$ at marginal stability and the dotted line is the first-order correction.

the development of the cells with anticlockwise motions in the figure whilst suppressing the motions and development in the cells with clockwise motions. It seems probable that as a result an amalgamation takes place between the pairs of cells in the very early stages of development. If this is so the cell heights which are observed should be twice those predicted, that is $2d(-2/R_z)^{\frac{1}{4}}$, or $2{\cdot}25d/(-R_z)^{\frac{1}{4}}$, where d is the width of the slot.

After their first growth, the rolls become less regular and generally larger by an amalgamation process similar to that described in the introduction for layers in a wide tank.

The results are presented in graphical form in figures 9 and 10.† Figure 9 shows a plot of $\log_{10}(-R_x)$ against $\log_{10}(-R_z)$. In the experiments,

$$R_{x'} = \frac{gd^4\beta S_{0x}}{\nu K_s} - \frac{gd^4\alpha\theta_{0x}}{\nu K_\theta},$$

is approximately equal to $gd^4\alpha\theta_{0x}/(\nu K_s)$, since $\beta S_{0x} = \theta_{0x}$ and $K_s \ll K_\theta$, and $R_z = gd^4\beta S_{0z}/(\nu K_s)$, since $\theta_{0z} = 0$. (We have taken the values

$$K_s = 1{\cdot}41 \times 10^{-5}\,\mathrm{cm^2\,sec^{-1}},$$

$$K_\theta = 1{\cdot}43 \times 10^{-3}\,\mathrm{cm^2\,sec^{-1}},$$

$$\nu = 1{\cdot}00 \times 10^{-2}\,\mathrm{cm^2\,sec^{-1}},$$

corresponding to 20 °C which was near the mean temperature of the experiments.)‡ The points indicate the values measured at the onset of instability and the vertical lines accompanying them indicate the probable range of errors introduced by the uncertainty of determining the exact temperature difference at which instability first occurs. The full curve represents the theoretical asymptotic curve for large $(-R_z)$, which has a slope of $\frac{5}{6}$, and the dotted curve indicates the first correction to this (see equation (A 9)). Agreement between the theory and observation is poor for points with $(-R_z) < 10^4$, but is good for higher values. Figure 10 shows a plot of the logarithm of the cell height divided by the slot width, against $\log_{10}(-R_z)$, and the full curve represents the theoretical asymptotic curve for large $(-R_z)$ on the assumption that the cell height is doubled as explained above. The dotted curve shows the first correction (see appendix A). The general trend of the theoretical curve is very well followed by the experimental points, but the observed cell heights are somewhat greater than those predicted. The maximum height to which a particle of fluid can rise in the initial density gradient, when heated by an amount equal to the temperature difference, $d\theta_{0x}$, between the plates, is $d\alpha\theta_{0x}/(\beta S_{0z})$. (This is the depth of the layers based on the explanation given by Mendenhall & Mason.) This height, divided

† A few additional experiments were made using sugar instead of salt to produce the initial density gradient. These experiments showed a trend towards the theoretical curve of figure 9, similar to that found using salt, but gave higher values for $(-R_x)$ by factors of 1·25 to 2 in the range $4{\cdot}25 < \log_{10}(-R_z) < 5{\cdot}25$. The values of cell heights were not distinguishable from those found using salt. Sugar has a coefficient of diffusivity of about $0{\cdot}52 \times 10^{-5}$ cm^2 sec^{-1}.

‡ The maximum salinities used in the experiments would produce an increase in viscosity of about 12 %.

by d, is equal to R_x/R_z. If the asymptotic relation $(-R_x) = 2{\cdot}76(-R_z)^{\frac{1}{3}}$ is valid, then this becomes $2{\cdot}76/(-R_z)^{\frac{1}{3}}$, which is not much different from the prediction for cell height divided by slot width given by our theory, and fits the observed values for cell height quite as well.

The general agreement between the observations and the theory at large values of $(-R_z)$ is surprising in view of the failure of the theory to observe the theoretical boundary conditions. It is known that, in the Bénard problem, the effect of different boundary conditions is to change considerably the critical Rayleigh numbers (see Chandrasekhar 1961, p. 43, table 3) and it therefore appears that the agreement found in our results is fortuitous. It is possible, however, that, since the ratio of height to width of the cells is becoming very small for large $(-R_z)$, the boundary conditions on the vertical walls play a small role in determining the cell motions and the onset of instability, provided that a condition of no flow through the walls is observed.

4. Experiments in a wide tank

Experiments have been performed to investigate the thermal and saline structures of the well-developed layers; further experiments with more refined apparatus could be performed to advantage, and the results given here should be taken as being essentially qualitative. The structure of the layers seemed to vary in detail between experiments, dependent mainly on the initial density gradient. A particular experiment, which appeared to be typical, is described here.

The layers were produced in a tank constructed of $\frac{1}{4}$ in. thick Perspex, measuring $10{\cdot}5 \times 10{\cdot}5 \times 20$ cm. A 2 mm thick brass wall separates the tank from a water bath containing an electric immersion heater, a stirrer and a thermometer. A linear salinity gradient was produced in the tank using the technique described by Oster (1965).

The electric immersion heater could be regulated using a Variac, and in these experiments a rapid initial rise in water bath temperature was aimed for, followed by a long period at a steady temperature once a horizontal temperature gradient had been established. In this experiment there was a rise to maximum temperature in about $1\frac{1}{2}$ min.

Cells were seen to develop rapidly, and more or less simultaneously throughout the height of the hot wall, in the form of two-dimensional rolls slightly inclined to the horizontal, eventually forming layers across the tank. The simplest method of visually observing the cells, and the developing layers, was found to be by noting the distortion of a vertical line of dye in the tank. Small crystals of potassium permanganate were dropped into the tank producing narrow vertical traces as they fell through the liquid. Currents towards the hot wall in the lower part of each layer and away from the hot wall in the upper part produce corresponding distortions in the dye line. These distortions were photographed, illumination being provided by a Photoflood light behind the tank, the light passing through a (water) heat-sink and an opal Perspex screen. The inferred maximum current speeds in the developed layers well away from the walls was

about 0·35 mm sec^{-1}. The upward currents near the hot wall and the downward currents near the cold wall were not estimated.

The initial density gradient was $1{\cdot}66 \times 10^{-3}$ g cm^{-4}, with the temperature of the hot wall being 11·25 °C above the initial temperature of the brine in the tank. The dimensions of the cells produced after 4 min as measured from a photograph are given in table 1 (*a*). A photograph of the well-developed layers about 72 min after the start is shown in figure 11, plate 2. The distorted dye pattern was dropped 80 sec before the photograph was taken. The hot wall is to the right and the scale at the left is in centimetres.

The vertical and horizontal profiles of temperatures and salinity were measured in the developing layers at various positions in the tank.

Salinity profiles were obtained from conductivity measurements. As standard precise methods of conductivity measurement are obviously not applicable to measurements at a point, the most satisfactory apparatus was found to be the single-electrode conductivity probe described by Gibson & Schwarz (1963). This gives an output dependent on the values of conductivity within a sphere of about 1 mm in diameter surrounding the fine tip of the probe. As only one small electrode need be moved about in the fluid (the earth can be left in one position), there is a minimum of disturbance to the cell system.

The probe and earth were placed in one arm of a Wayne Kerr High Precision Comparator. The ratio of the comparator was left at 1·000, and the impedance of the probe balanced by a resistance box and capacitance box in parallel in the other arm. For a traverse the impedance is roughly balanced, and changes in the resistance of the probe circuit are measured by putting the out-of-balance signal through a u.v. recorder. As the out-of-balance signal is non-linear with relation to the conductivity at the probe tip, a suitable calibration curve was plotted, and u.v. records used in conjunction with this to give the final profiles. Temperature corrections to the conductivity were made for some salinity profiles, and were found to be insufficient to alter the basic shape of the salinity curves.

The temperature profiles were obtained by means of a 200 Ω nominal resistance thermistor mounted at the end of $\frac{1}{4}$ in. diameter glass tube. This could replace the conductivity probe and earth in the arm of the comparator, the final output being obtained in an identical manner. In later experiments a d.c. thermistor bridge circuit was used. The thermistor and conductivity probes could then be strapped together, allowing simultaneous values of temperature and conductivity at a point to be measured on the u.v. recorder.

Both conductivity probe and thermistor assembly could be mounted on a carriage which could be wound by hand vertically up and down in the tank. As the output of the u.v. recorder is time-based, this could only be converted to a depth co-ordinate if the rate of winding the handle was reasonably constant throughout the traverse. In table 1, the measurements (*a*) are taken by noting the position in each cell at which the current velocity, as indicated by the distortion of a line of dye, towards the hot wall is a maximum. Measurements (*b*) are obtained from a vertical temperature traverse taken at the same time as the photograph (time taken for traverse about 60 sec). The position in each cell at

which the temperature is a minimum was noted, and the cell heights calculated assuming a constant vertical velocity of the thermistor throughout the traverse. It would appear from these results that the velocity of traverse was reasonably constant throughout most of the traverse, and attempts to synchronize the winding rate with a stop-watch were found to be reasonably successful.

Cell	*A*	*B*	*C*	*D*	*E*
(*a*)	0·96	1·27	0·77	0·73	0·73
(*b*)	0·93	1·24	0·79	0·74	0·65

TABLE 1. Heights in cm of 5 cells after 4 min. (*a*) As measured directly from a photograph. (*b*) As measured from a vertical temperature traverse

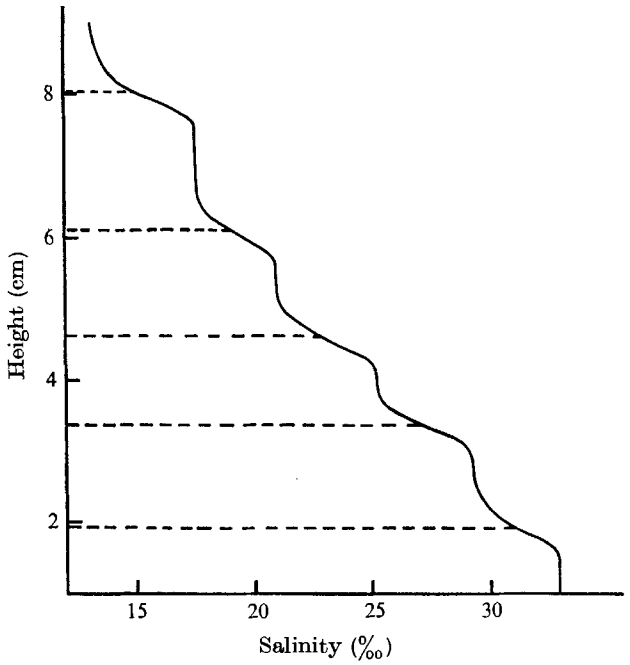

FIGURE 12. The vertical salinity profile near the hot wall, 170 min after the start of the experiment. By this time the layers were well developed right across the tank. The dotted lines indicate the positions of the cell boundaries.

A similar carriage was set up to perform horizontal traverses of the thermistor and probe.

Typical vertical traverses for salinity and temperature can be seen in figures 12 and 13. Approximate positions of the cell boundaries are indicated.

From figure 12 it can be seen that the salinity is more or less constant throughout a fair proportion of the cell height, indicating mixing within the cells. The initial linear salinity profile becomes stepped as the liquid takes on a layered structure.

Figure 13 indicates that the temperature at the top of the cell is greater than at the bottom, as would be expected, though a certain amount of mixing appears to take place at the cell boundaries. The mechanism of mixing at the cell boundaries was not clear, but in the well-developed layers there frequently appeared to be narrow pencils of fluid, when coloured by dye, which looked very similar to salt fingers. These seemed to originate at the cell boundaries, where they sometimes had the appearance of cusped waves (see Thorpe 1968, figure

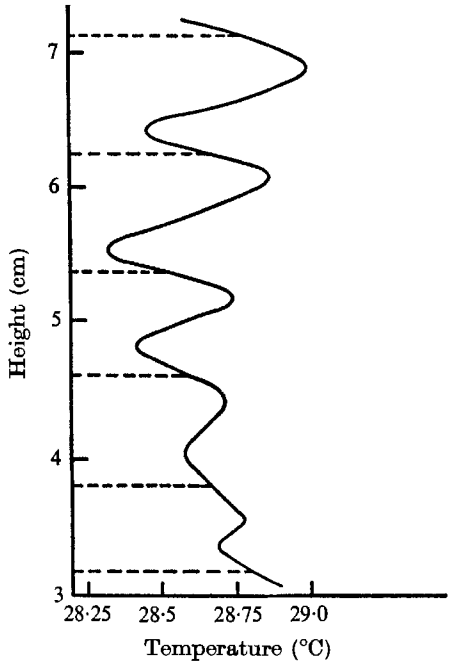

FIGURE 13. The vertical temperature profile near the hot wall, 4 min after the start of the experiment. The dotted lines indicate the positions of the cell boundaries.

3(*a*)). The mean temperature of the cells increases towards the bottom of the tank. This effect may be caused by the development of a cell at the bottom of the tank which is rather deeper than those above it. This cell is the first to form (probably in the manner described by Mendenhall & Mason 1923) and, having a greater area in contact with the hot wall, is probably more effective in transporting heat than cells at a higher level.

Horizontal traverses show a steady, almost linear, increase in temperature approaching the hot wall once a steady state has been reached, and a similar horizontal increase in salinity towards the hot wall is also noticed. From the horizontal and vertical traverses some idea of the temperature and salinity fields in the well-developed layers can be obtained. These are shown diagrammatically in figures 14(*a*) and (*b*).

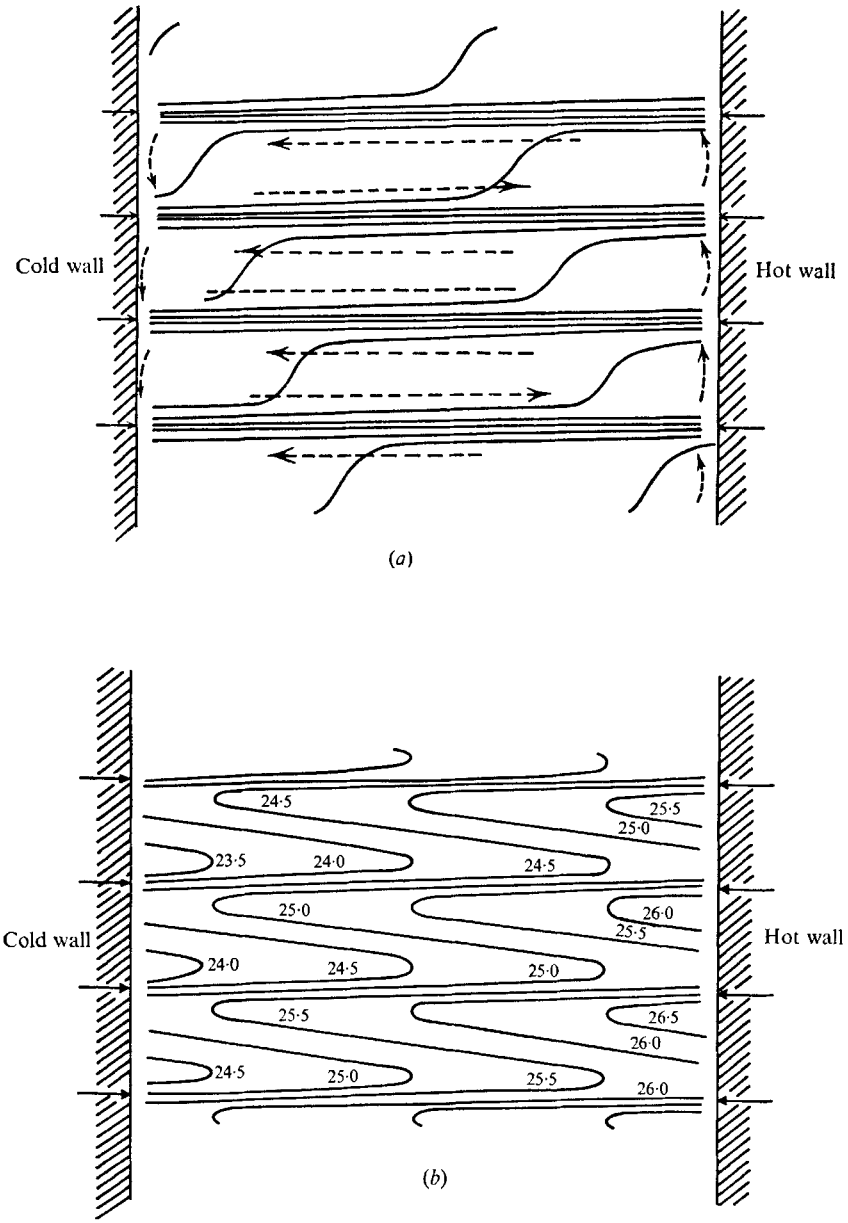

FIGURE 14. (*a*) The salinity field in a vertical plane along the tank after 170 min shown diagrammatically. The isohalines are at 0·5 ‰ intervals with salinity increasing downwards everywhere, and the dotted arrows indicate the directions of the mean fluid motions. The arrows at the walls indicate the layer boundaries. The vertical scale is exaggerated $5\frac{1}{2}$ times. (*b*) The corresponding temperature field. The isotherms are drawn at 0·5 °C intervals.

5. Final remarks and conclusions

We have examined the possibility of instability of a steady convective nature arising from the presence of horizontal salinity and temperature gradients in a stably stratified fluid, and compared the theoretical results with an experiment in a narrow vertical slot. The results of the analysis are applied to a fluid bounded by parallel planes which may be vertical (corresponding to the experimental situation) or horizontal (as in the Bénard problem). Relations between a parameter based on horizontal gradients (R_x) and a parameter based on vertical gradients (R_z) are found, which describe the conditions of marginal stability in situations in which realistic boundary conditions are not satisfied. Good agreement is found between the theoretical predictions and observations, and it is suggested that this is not fortuitous, but the result of the particular cell structure.

A complete solution of the problem would include not only more realistic boundary conditions, but also a search for overstable modes of instability. It appears (from analyses not presented here) that overstability will occur in the presence of horizontal gradients if it can occur in the equivalent situations in their absence, but it is not clear if and when the overstable mode will occur before the convective mode. In the experiments, which have a stable salt gradient and no vertical temperature gradient, no growing oscillations were observed, and the onset of instability appeared to be due to steady convective motions.

It is suggested that the layers, which are observed to grow simultaneously in a broad tank containing stratified brine solution when the walls are heated (figure 1), arise from the development of instability of this nature in the neighbourhood of the heated walls, where conditions occur which are similar to those found in the slot. The actual scale of the layers when they first develop will depend upon the heating rates, as explained in the introduction.

Stern (1967) has suggested that a mechanism of instability due to the presence of horizontal gradients in the ocean may account for some of the layers which have been found, sometimes at quite considerable depths, in many parts of the World's oceans (see, for examples, Stommel & Fedorov 1967; Tait & Howe 1968). The layers have typical thicknesses of 10 m and are separated by quite thin interfaces, probably about 1 m on average. The horizontal extent of single layers is possibly 10 km or more. Almost compensating horizontal gradients of temperature and salinity are known to exist in some of the layers (Tait, private communication) and are found not uncommonly in the ocean (see, for examples, Stommel & Fedorov 1967; Mann 1967). This paper lends support to the ideas developed by Stern that layers may develop in the ocean in the presence of horizontal gradients and, whilst it is impossible to estimate exactly the vertical scale of the layers, it would seem that a few metres would not be unreasonable if our results can be carried over to a large scale. Once developed, the layers may be maintained by salt-fingering processes as suggested by Turner (1968). A knowledge of the mean velocity field in the oceanic layers would go a long way towards establishing whether their generation could be due to the mechanism discussed here, and instruments are now being developed for making such measurements.

Appendix A

When $\gamma = \frac{1}{2}\pi$ from (15) we have

$$[(L \mp 1)^2 + M^2]^3 = R_z(L \mp 1)^2 - R_x M(L \mp 1), \tag{A 1}$$

from which we require the minimum value of $|R_x|$ for given R_z.

$$(a) \quad -R_z \gg 1$$

By adding and subtracting equations (A 1) we obtain

$$2LR_z - MR_x = 2L[3(L^2+M^2+1)^2 + 4L^2], \tag{A 2}$$

$$(1+L^2)R_z - LMR_x = (L^2+M^2+1)[(L^2+M^2+1)^2 + 12L^2]. \tag{A 3}$$

Clearly, if $(-R_z)$ is large, either $|L| \gg 1$ or $|M| \gg 1$ (or both), and so retaining only the leading terms in (A 2) and (A 3)

$$2LR_z - MR_x = 6L(L^2+M^2)^2, \tag{A 4}$$

$$(1+L^2)R_z - LMR_x = (L^2+M^2)^3. \tag{A 5}$$

Eliminating R_x, we have

$$(L^2-1)R_z = (5L^2-M^2)(L^2+M^2)^2. \tag{A 6}$$

Put $x = L^2+M^2$ so that (A 6) gives $L^2 = (R_z - x^3)/(R_z - 6x^3)$. If we choose our frame of reference so that $L, M > 0$ we have

$$M = (x-L^2)^{\frac{1}{2}} = \left(\frac{5x^3 - xR_z + R_z}{6x^2 - R_z}\right)^{\frac{1}{2}},$$

and so, by substitution in (A 4)

$$R_x = 2(R_x - 3x^2)\left(\frac{x^3 - R_z}{5x^3 - xR_z + R_z}\right)^{\frac{1}{2}}. \tag{A 7}$$

It may be shown by differentiation that R_x has a stationary value at $x = (-\frac{1}{2}R_z)^{\frac{1}{2}}$, which gives a minimum value for $(-R_x)$ of $2{\cdot}76(-R_z)^{\frac{5}{6}}$. The corresponding values of L and M are approximately

$$L = \sqrt{(\tfrac{3}{2})}, \quad M = (-\tfrac{1}{2}R_z)^{\frac{1}{6}}. \tag{A 8}$$

The next-order terms may be found by solving the equations

$$2LR_z - MR_x = 6LM^4,$$

$$(1+L^2)R_z - LMR_x = M^6 + 3M^4(1+L^2),$$

which gives a minimum value

$$(-R_x) = 2{\cdot}76(-R_z)^{\frac{5}{6}}[1 + 1{\cdot}56(-R_z)^{-\frac{1}{3}}], \tag{A 9}$$

when

$$L = \sqrt{(\tfrac{3}{2})}[1 + 2{\cdot}19(R_z)^{-\frac{1}{3}}], \tag{A 10}$$

and

$$M = (-\tfrac{1}{2}R_z)^{\frac{1}{6}}[1 - (-\tfrac{1}{2}R_z)^{-\frac{1}{3}}], \tag{A 11}$$

approximately.

(*b*) $R_z = 0$

In this case (A 2) and (A 3) reduce to

$$-MR_x = 2L[3(L^2+M^2+1)^2+4L^2], \tag{A 12}$$

$$-LMR_x = (L^2+M^2+1)[(L^2+M^2+1)^2+12L^2]. \tag{A 13}$$

The substitution $\alpha = (L^2+M^2+1)/L^2$, $\beta = 4/L^2$, and subsequent elimination of β yield

$$(-R_x) = \frac{512(3\alpha-2)^{\frac{3}{2}}}{\alpha(6-\alpha)^2(\alpha-2)^{\frac{1}{2}}(\alpha^2+8\alpha-4)^{\frac{1}{2}}} \quad \text{if} \quad 2 \leqslant \alpha \leqslant 6.$$

This has a minimum for $|R_x|$ at $\alpha = 2{\cdot}7$ approximately, and at this minimum $(-R_x) = 63$, $M = 0{\cdot}84$, $L = 1{\cdot}01$ approximately.

Appendix B

For the horizontal layer $\gamma = 0$, we need to minimize for $|R_x|$ the equations

$$[L^2+(M\pm 1)^2]^3+R_xL(M\pm 1)-R_zL^2 = 0, \tag{B 1}$$

which may be written

$$L^2R_z-MLR_x = (L^2+M^2+1)[(L^2+M^2+1)^2+12M^2], \tag{B 2}$$

$$-LR_x = 2M[3(L^2+M^2+1)^2+4M^2]. \tag{B 3}$$

(*a*) $-R_z \gg 1$

Suppose $$R_x \sim (-R_z)^\alpha, \quad L/M \sim (-R_z)^\beta,$$

then from (B 2), (B 3), $\alpha-\beta \geqslant 0$, and $\alpha+\beta \geqslant 0$, and so $\alpha \geqslant \frac{1}{2}$. Since we are looking for a minimum value of R_x, we try $\alpha = \frac{1}{2}$ and then $\beta = -\frac{1}{2}$, $M \gg L$. By neglecting L in comparison with M, and eliminating L we find, from (B 2) and (B 3)

$$(-R_x) = (-R_z)^{\frac{1}{2}}\frac{2M(3M^4+10M^2+3)}{(5M^6+5M^4-9M^2-1)^{\frac{1}{2}}}.$$

This has a minimum value when $M = 1{\cdot}4$ and

$$(-R_x) = 15{\cdot}6(-R_z)^{\frac{1}{2}}, \quad L = 6{\cdot}2(-R_z)^{-\frac{1}{2}}, \quad \text{approximately.}$$

(*b*) $R_z = 0$

The equations now are exactly the same as the case $\gamma = \frac{1}{2}\pi$, and so at the minimum $(-R_x) = 63$ and $L = 1{\cdot}01$, $M = 0{\cdot}84$.

Appendix C

In the earlier analysis we supposed that the motion was two-dimensional. We now show that the effect of introducing a dependence on the y direction is to increase the horizontal parameter $|R_x|$, so that the *first* unstable mode is two-dimensional.

The steady perturbation equations are

$$\nu\nabla^4\boldsymbol{\omega} = g\left[\frac{\partial}{\partial y}(\beta S-\alpha\theta), \quad -\frac{\partial}{\partial x}(\beta S-\alpha\theta), \quad 0\right], \tag{C 1}$$

$$u\theta_{0x}+\omega\theta_{0z} = K_\theta\nabla^2\theta, \tag{C 2}$$

$$uS_{0x}+\omega S_{0z} = K_s\nabla^2 S, \tag{C 3}$$

$$\nabla.\mathbf{u} = 0. \tag{C 4}$$

Since, from (C 1), $$\nabla^2\left(\frac{\partial u}{\partial y}-\frac{\partial u}{\partial x}\right) = 0,$$

we can write $\nabla^2 u = \phi_x$, and $\nabla^2 v = \phi_y$. From (C 4) we have

$$\nabla^2\omega_z = -\nabla_1^2\phi,$$

where $$\nabla_1^2 \equiv \frac{\partial^2}{\partial x^2}+\frac{\partial^2}{\partial y^2}.$$

By eliminating θ and S from (C 1), (C 2), (C 3) we find

$$\nabla^4(-\nabla^2\phi_y, \nabla^2\phi_x, 0) = \left[\frac{\partial\Phi}{\partial y}, \frac{\partial\Phi}{\partial x}, 0\right], \tag{C 5}$$

where $$\Phi = \frac{g}{\nu}\left(\beta\frac{S_{0x}}{K_s}-\frac{\alpha\theta_{0x}}{K_\theta}\right)\phi_{xz}-\frac{g}{\nu}\left(\beta\frac{S_{0z}}{K_s}-\alpha\frac{\theta_{0z}}{K_\theta}\right)\nabla_1^2\phi, \tag{C 6}$$

and so $$\nabla^6\phi+\Phi = f(z),$$

where $f(z)$ is an arbitrary function of z.

A solution corresponding to (13) is

$$\phi = \phi^{(+)}\cos[(k+l)x-(k\cot\gamma-m)z]\sin qy + \phi^{(-)}\cos[(k-l)x-(k\cot\gamma+m)z]\sin qy,$$

where $$\phi^{(\pm)} = \frac{2(k\cot\gamma\mp m)}{(k\pm l)^2+q^2}[(k\pm l)^2+(k\cot\gamma\mp m)^2+q^2],$$

and this satisfies (C 6) if

$$[(L\mp 1)^2+(M\pm\cot\gamma)^2+Q^2]^3 = R_z[(L\mp 1)^2+Q^2]-R_x[L\mp 1][M\pm\cot\gamma], \tag{C 7}$$

where L, M, R_x, R_z are as defined before (see equation (15)), and $Q = qd/(n\pi\sin\gamma)$. These equations are equivalent to

$$(p_1^2+q^2+Q^2)^3 = R_z(p_1^2+Q^2)-R_x p_1 q_1, \tag{C 8}$$

with origins displaced to $(-1, \cot\gamma)$ and $(1, -\cot\gamma)$ in the (p_1, q_1) plane.

It may easily be shown that the set of curves (C 8) for $Q \neq 0$ lie inside the curve, given by (17), for which $Q = 0$. Hence the minimum value of $|R_x|$ at which the two curves (C 7) touch, and have a common root, is that at which $Q = 0$. Hence, for the type of solutions considered, the onset of instability is characterized by no y dependence, and motions have the form of two-dimensional rolls.

REFERENCES

CHANDRASEKHAR, S. 1961 *Hydrodynamic and Hydromagnetic Stability*. Oxford University Press.

CURRIE, I. G. 1967 *J. Fluid Mech.* **29**, 337.

GIBSON, C. H. & SCHWARZ, W. H. 1963 *J. Fluid Mech.* **16**, 357.

MANN, C. R. 1967 *Deep Sea Res.* **14**, 337.

MENDENHALL, C. E. & MASON, M. 1923 *Proc. Natn. Acad. Sci.* **9**, 199.

NIELD, D. A. 1967 *J. Fluid Mech.* **29**, 545.

OSTER, G. 1965 *Sci. American*, **212**, 70.

STERN, M. 1960 *Tellus*, **12**, 172.

STERN, M. 1967 *Deep Sea Res.* **14**, 747.

STOMMELL, H. & FEDOROV, K. N. 1967 *Tellus*, **19**, 306.

TAIT, R. I. & HOWE, M. R. 1968 *Deep Sea Res.* **14**, 275.

THORPE, S. A. 1966 Ph.D. Thesis. University of Cambridge.

THORPE, S. A. 1968 *J. Fluid Mech.* **32**, 693.

TURNER, J. S. 1967 *Deep Sea Res.* **14**, 599.

TURNER, J. S. 1968 *J. Fluid Mech.* **33**, 183.

TURNER, J. S. & STOMMEL, H. 1964 *Proc. U.S. natn. Acad. Sci.* **52**, 49.

VERONIS, G. 1965 *J. Mar. Res.* **23**, 1.

WALIN, G. 1964 *Tellus*, **16**, 389.